Eur Radiol (2017) 27:454–463
DOI 10.1007/s00330-016-4382-7

MUSCULOSKELETAL

C-arm flat-panel CT arthrography of the shoulder: Radiation dose considerations and preliminary data on diagnostic performance

Roman Guggenberger[1] · Erika J. Ulbrich[1] · Tobias J. Dietrich[2] · Rosemarie Scholz[3] · Pascal Kaelin[1] · Christoph Köhler[3] · Thilo Elsässer[3] · Thomas Le Corroller[4,5] · Thomas Pfammatter[1] · Hatem Alkadhi[1] · Gustav Andreisek[1]

Received: 10 August 2015 / Revised: 19 April 2016 / Accepted: 25 April 2016 / Published online: 24 May 2016

Abstract

Objectives To investigate radiation dose and diagnostic performance of C-arm flat-panel CT (FPCT) versus standard multi-detector CT (MDCT) shoulder arthrography using MRI-arthrography as reference standard.

Methods Radiation dose of two different FPCT acquisitions (5 and 20 s) and standard MDCT of the shoulder were assessed using phantoms and thermoluminescence dosimetry. FPCT arthrographies were performed in 34 patients (mean age 44 ± 15 years). Different joint structures were quantitatively and qualitatively assessed by two independent radiologists. Inter-reader agreement and diagnostic performance were calculated.

Results Effective radiation dose was markedly lower in FPCT 5 s (0.6 mSv) compared to MDCT (1.7 mSv) and FPCT 20 s (3.4 mSv). Contrast-to-noise ratios (CNRs) were significantly ($p < 0.05$) higher in FPCT 20-s versus 5-s protocols. Inter-reader agreements of qualitative ratings ranged between $\kappa = 0.47–1.0$. Sensitivities for cartilage and rotator cuff pathologies were low for FPCT 5-s (40 % and 20 %) and moderate for FPCT 20-s protocols (75 % and 73 %). FPCT showed high sensitivity (81–86 % and 89–99 %) for bone and acromioclavicular-joint pathologies.

Conclusion Using a 5-s protocol FPCT shoulder arthrography provides lower radiation dose compared to MDCT but poor sensitivity for cartilage and rotator cuff pathologies. FPCT 20-s protocol is moderately sensitive for cartilage and rotator cuff tendon pathology with markedly higher radiation dose compared to MDCT.

Key Points

- *FPCT shoulder arthrography is feasible with fluoroscopy and CT in one workflow.*
- *A 5-s FPCT protocol applies a lower radiation dose than MDCT.*
- *A 20-s FPCT protocol is moderately sensitive for cartilage and tendon pathology.*

Keywords Computed tomography · Radiation dose · Arthrography · Shoulder · C-arm cone-beam CT

Electronic supplementary material The online version of this article (doi:10.1007/s00330-016-4382-7) contains supplementary material, which is available to authorized users.

✉ Roman Guggenberger
Roman.Guggenberger@usz.ch

[1] Institute of Diagnostic and Interventional Radiology, University Hospital Zurich, Rämistrasse 100, 8091 Zürich, Switzerland

[2] Department of Radiology, Balgrist University Hospital, Zurich, Switzerland

[3] Siemens Healthcare GmbH, Business Area Advanced Therapies, Forchheim, Germany

[4] Aix-Marseille Université, CNRS, ISM UMR 7287, Marseille, France

[5] Radiology Department, APHM, Marseille, France

Introduction

Computed tomography (CT) arthrography of the shoulder is considered an accurate tool for the evaluation of the glenohumeral joint including rotator cuff muscles and tendons, joint capsule, the glenoid labrum and articular cartilage [1, 2]. It is usually performed preoperatively in order to quantify glenoid bone loss after joint luxation or as an alternative to contraindications for MR-imaging, e.g. cardiac pacer, claustrophobia or large metallic implants. The typical set-up for CT

arthrography includes intra-articular injection of iodinated contrast material either with ultrasonography, flat-panel (FP) or CT fluoroscopy, followed by multidetector computed tomography (MDCT) arthrography [3].

>In the past few years, various vendors have equipped fluoroscopy units with robotic C-arms and digital FP detector technology. By automatic rotation of the C-arm around the patient while acquiring a predefined number of 2D projections, a volumetric dataset is obtained allowing for multiplanar reconstructions in arbitrary planes analogous to MDCT [4]. Due to cone beam x-ray geometry in combination with planar detector technology, these systems potentially provide higher spatial resolution compared with MDCT [5, 6]. In addition so-called multi-axis C-arm systems allow eccentric rotations to specifically image peripheral parts of the body, hereby keeping the structure of interest within the isocentre of the C-arm trajectory [7]. Hence, FPCT arthrography of the shoulder is now possible with prior intra-articular contrast injection under fluoroscopic guidance followed by volumetric tomography using the same modality without relocating the patient [8, 9].

There are several technical aspects that would argue for FPCT arthrography. In order to decrease image noise, increase rotation speed and maintain a good signal-to-noise (SNR) and contrast-to-noise (CNR) ratio adjacent detector elements are usually grouped together ('binning') in FPCT [10]. In addition, FPCT normally operates at higher bit depths than MDCT, offering larger gray scales [11, 12] potentially increasing image contrast [13, 14]. Since tube voltage used in FPCT is generally lower than in MDCT (70 kV vs. 100–40 kV, respectively), the resulting iodine contrast may increase and radiation doses decrease. The latter would be of particular interest given the proximity of the shoulder to radiosensitive organs such as the thyroid gland but is hampered by the difficulty of directly comparing the dose area product (DAP) from FPCT with the dose length product (DLP) from MDCT, unless dedicated phantom measurements are performed [15].

Therefore, we have designed a study to investigate: first, the radiation dose of both FPCT and MDCT arthrography of the shoulder in vitro using thermo-luminescence dosimetry (TLD) in an anthropomorphic Rando-Alderson phantom, and second, to prospectively investigate as proof of concept the feasibility and diagnostic performance of FPCT arthrography in vivo in patients using MR arthrography as the reference standard.

Materials and methods

This prospective study was approved by the local ethics board. Written informed consent was obtained from all patients.

In vitro investigations

Rando-Alderson-phantom and thermoluminescence dosimeter (TLD) measurements

All acquisitions were performed on the right shoulder of an anthropomorphic Rando-Alderson phantom. A detailed description of this phantom is given by Deak et al. [16] and Archer et al. [17]. Multiple predefined drill holes (5 mm) allow for insertion of lithium fluoride (LiF) thermoluminescence dosimeters (TLDs) and, thus, highly accurate dose measurements of certain body regions of the trunk (Table 1). Additional holes in the shoulder were drilled to host TLD rods allowing for side-to-side comparisons. Radiation dose measurements were performed by the vendor of the FPCT unit according to a rigidly defined, internally standardized protocol. This had been tested prior and proven to deliver robust and reproducible dose measurements (see also Supplemental Material). Based on the mean absorbed radiation dose (mGy) of the TLDs, respective effective organ and total body doses (mSv) were calculated using specific tissue-weighting factors according to the ICRP 103 recommendations [18].

In vitro FPCT data acquisition

Phantom acquisitions were performed on a FPCT scanner (Artis zeego, Siemens Healthcare, Forchheim, Germany) with a C-arm-mounted FP detector (30 cm × 40 cm). The FP detector was operated at a standard 2 × 2 binning mode, meaning four adjacent detector elements were grouped and read out together. Two FPCT acquisition protocols were applied: first, a fast 5-s, lower radiation dose protocol using vendor-specific default pre-settings; second, a slower (20-s), higher radiation dose protocol using vendor-modified pre-settings which allowed in analogy to the 5-s acquisition for a rotation of the C-arm around an eccentric isocentre , i.e. the shoulder joint . Thus, both acquisitions were potentially subject to the same truncation artefacts associated with eccentric rotations. Compared to the standard setting, the radiation dose was reducedl from 1.2 μGy/frame to 0.36 μGy/frame in 20-s acquistions. The FPCT 5-s and 20-s acquisitions were both operated at 70 kVp with automated exposure control. Different angulation steps (1.5° and 0.4°, respectively) lead to different numbers of projections (133 and 500, respectively) and different acquisition durations for the standard 200° rotation of the C-arm around the patient. Focal spot size was small for both acquisitions. Mean estimated tube voltage, tube current and pulse width as noted from the respective in vivo exam protocols were 80.9 ± 5.03 kVp, 272.2 ± 70.6 mA and 6.9 ± 1.8 ms for 5-s acquisitions, respectively. The corresponding values for the 20-s runs were 82.4 ± 4.2 kVp, 260.6 ± 30.6 mA and 7.7 ± 1.7 ms. Equal collimation for both acquisitions was used:

Table 1 In vitro radiation dose measurements. Mean organ dose values (in mSv) of different acquisition protocols in vitro

	FPCT 5 sec	FPCT 20 sec	MDCT	p-value		
	Mean Organ Dose (± SD)	Mean Organ Dose (± SD)	Mean Organ Dose (± SD)	FPCT 5 s vs. FPCT 20 s	FPCT 5 s vs. MDCT	FPCT 20 s vs. MDCT
Shoulder right	10.50 (±3.15)	79.29 (±30.32)	7.82 (± 1.71)	0.000*	0.000*	0.000*
Shoulder left	9.01 (± 4.55)	9.59 (± 4.66)	7.34 (± 1.58)	0.657	0.094	**0.030**
Brain	0.09 (± N/A)	0.35 (± N/A)	0.11 (± N/A)	N/A	N/A	N/A
Thyroid gland	2.41 (± N/A)	10.03 (± N/A)	3.78 (± N/A)	N/A	N/A	N/A
Lung right	2.37 (± 1.86)	14.31 (± 11.37)	4.78 (± 3.13)	**0.009**	**0.050**	**0.028**
Lung left	1.65 (± 1.68)	7.07 (± 5.54)	4.76 (± 2.90)	**0.013**	**0.009**	0.264
Sternum	1.81 (± 0.33)	15.71 (± 0.57)	10.85 (± 2.81)	N/A	N/A	N/A
Thymus	2.46 (± N/A)	16.35 (± N/A)	8.52 (± N/A)	N/A	N/A	N/A
Oesophagus	2.93 (± N/A)	16.36 (± N/A)	4.86 (± N/A)	N/A	N/A	N/A
Liver	0.09 (± 0.05)	0.39 (± 0.28)	0.32 (± 0.23)	**0.029**	0.052	0.664
Stomach	0.06 (± 0.03)	0.17 (± 0.08)	0.26 (± 0.08)	N/A	N/A	N/A
Adrenal gland	0.04 (± N/A)	0.08 (± N/A)	0.28 (± N/A)	N/A	N/A	N/A
Pancreas	0.04 (± N/A)	0.20 (± N/A)	0.29 (± N/A)	N/A	N/A	N/A
Kidney	0.03 (± N/A)	0.21 (± N/A)	0.14 (± N/A)	N/A	N/A	N/A
Spleen	0.04 (± N/A)	0.10 (± N/A)	0.15 (± N/A)	N/A	N/A	N/A
Small intestine	0.00 (± N/A)	0.00 (± N/A)	0.05 (± N/A)	N/A	N/A	N/A
Large intestine	0.00 (± N/A)	0.00 (± N/A)	0.04 (± N/A)	N/A	N/A	N/A
Urinary bladder	0.01 (± N/A)	0.00 (± N/A)	0.04 (± N/A)	N/A	N/A	N/A
Testes	- 0.02 (± N/A)	0.14 (± N/A)	0.01 (± N/A)	N/A	N/A	N/A

SD standard deviation; *TLD* thermoluminescent dosimeter, *FPCT* flat-panel computed tomography, *MDCT* multidetector computed tomography, *N/A* not available

Significant p-values are given in bold; if significant when corrected for alpha-error of multiple comparisons (Bonferroni correction: $0.05/19 \leq 0.003$) marked with an asterisk (*)

cranio-caudal collimation was chosen at the iso-centre in order to approximate the scan length of a standard CT scan of the shoulder joint starting from 1 cm above the acromio-clavicular joint to about 3 cm caudal to the humeral head. The applied dose at the interventional reference point (IRP) in mGy and the dose area product (DAP) given by the scanner were noted and compared to radiation doses measured with TLDs.

In vitro multidetector computed tomography (MDCT) data acquisition

Multidetector CT acquisitions were performed on a 128-slice CT scanner (SOMATOM Definition Flash; Siemens Healthcare, Forchheim, Germany) using the clinical standard protocol of our institution according to reported acquisition and radiation dose parameters [19]: tube voltage, 120 kVp;

tube current-time product, 167 effective mAs per rotation using automated attenuation-based tube current modulation (CARE Dose 4D, Siemens); pitch, 0.85; detector collimation, 16 × 0.3 mm. The volume computed tomography dose index ($CTDI_{vol}$) given by the scanner was noted and compared to radiation doses as measured with TLDs.

In vivo investigations

Patients

For the in vivo assessment, patients who were referred for MR arthrography were asked for their written informed consent to participate in this study. For all subjects, inclusion criteria included: age > 18 years, written informed consent and referral for MR arthrography. Exclusion criteria included age < 18 years, hypersensitivity to iodinated contrast media, nephropathy with an estimated glomerular filtration rate <30 ml/min, pregnancy, current infection of the shoulder and metallic implants. Potential metal-induced artifacts in FPCT would have hampered qualitative readouts and were beyond the scope of this proof of concept study. From 38 subjects, two patients were excluded due to artifacts in FPCT (sedimentation of intra-articular iodine contrast) and two patients due to artifacts in MR arthrography (movement artifacts). Thus, 34 patients (11 female, mean age 44 ± 15.0 years; age range 19–63 years) were finally included in this study. Seventeen patients were randomized to the FPCT 5-s protocol (mean age 36.3 ± 15.0 years; age range 19–63 years), the remainder to the FPCT 20-s protocol (mean age 31.1 ± 6.9 years; age range 21–43 years) . Medical indications for MR arthrography were moderate to severe shoulder trauma (n = 9), dislocated shoulder (n = 11), chronic shoulder pain (n = 6), impaired mobility of the shoulder (n = 4) and suspected rotator cuff lesion (n = 4).

Flat-panel CT (FPCT) and MR arthrography data acquisition

Shoulder joints were injected in the rotator interval under fluoroscopic guidance according to a standardized procedure using 1 ml of local anaesthetic, followed by a mixture of 3 ml of iodinated contrast agent (iopromide, Ultravist 300 mg iodine/ml Bayer Healthcare, Berlin, Germany) and 5 ml of gadolinium contrast agent (gadoteric acid, Artirem 0.0025 mmol gadolinium/ml, Guerbet Group, Villepinte, France). Hence, concentration of iodine in the injected solution was 100 mg iodine/ml leading to an expected intra-articular concentration of about 80 mg iodine/ml according to previous studies [8, 14]. Although iodine may impact on the SNR of gadolinium-enhanced MR arthrography, the effect may be negligible at an intra-articular iodine concentration of 80 mg iodine/ml [20]. Both fluoroscopy and FPCT acquisitions were performed on the same unit (Artis zeego, Siemens Healthcare, Forchheim, Germany) using equal acquisition parameters as used in the in vitro acquisitions (Fig. 1).

Following contrast injection, all patients underwent MR arthrography at 1.5 T (Signa EXCITE HDx, GE Healthcare, Waukesha, WI, USA) of the affected shoulder within a maximum of 30 min using a dedicated 8-channel shoulder coil (Neocoil, Pewaukee, WI, USA) and the standard MR acquisition protocol of our institution (Supplemental Table 1).

Postprocessing and image analysis

All FPCT data were transferred to a separate workstation (syngo X Workplace, Siemens) and postprocessed using dedicated software (InSpace 3D, Siemens). Axial thin-slice images were reconstructed by applying a bone-kernel at 10 × 10 cm field of view and 512 × 512 matrix size. This resulted in an isotropic voxel size of 0.29 mm. Multiplanar reformations (MPRs) in axial, coronal and sagittal planes were produced using a slice thickness of 1 mm, and an increment of 0.6 mm. The MPR images were then transferred to the picture

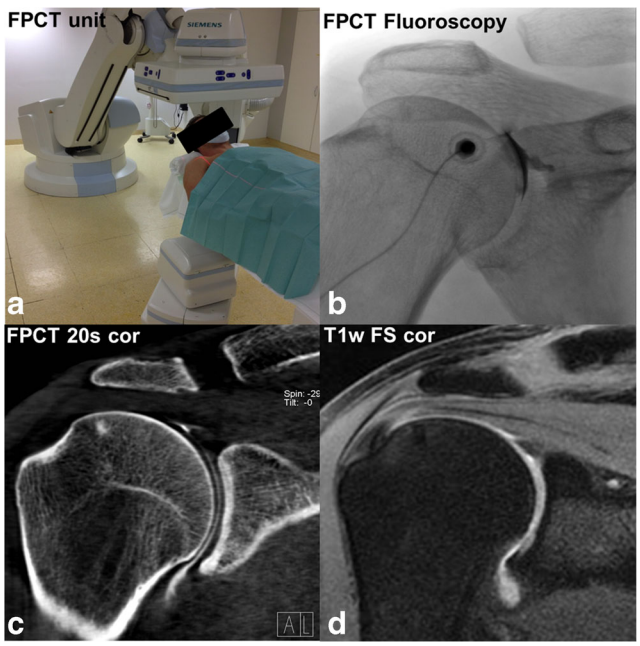

Fig. 1 Twenty-nine-year-old male patient lying supine on the examination table of the roboter arm mounted C-arm flat panel CT (FPCT) unit with the right shoulder in the isocentre of the eccentric C-arm rotation trajectory (**a**). After fluoroscopically guided contrast injection (**b**) FPCT 20-s arthrography of the right shoulder was performed in the same unit (**c**, coronal reformat). Patient underwent MR arthrography of the same shoulder joint immediately after FPCT (**d**, T1-weighted fat saturated (FS) coronal image). Normal glenohumeral joint with intact supraspinate tendon is visualized in both modalities

archiving and communication system (PACS) of our hospital (IMPAX 6, Agfa-Gevaert N.V., Belgium).

Quantitative image analysis

Quantitative measurements were performed by one reader (P.K.) with 3 years of experience in MSK imaging after a thorough instruction on a test data set not used for diagnostic read-out. Regions of interest (ROIs) with predefined areas (3, 6, 100 and 50 mm^2 for articular cartilage, labrum, bone/muscle and joint space, respectively) were placed at predefined locations of the shoulder joint in order to measure average attenuation in Hounsfield units (HU), noise (standard deviations of HU) and CNRs. For more detailed description refer to the Supplemental Material.

Qualitative image analysis

FPCT shoulder arthrographies were both separately and in consensus evaluated by two independent fellowship-trained readers (R.G. and E.U.) with 6 and 9 years of experience in musculoskeletal imaging, respectively, who were blinded to clinical data and acquisition protocol. Technical quality of intra-articular contrast injection and overall depiction quality of articular structures were rated on a 3-point Likert scale (1 = perfect, 2 = moderate and 3 = poor technical quality, image artifacts and depiction quality of structures).

In addition, pathological changes on either humeral or glenoid cartilage, bone, glenoid labrum including insertion and course of biceps tendon, rotator cuff tendons, and acromioclavicular joint were rated on a modified 3-point nominal scale based on traditional grading scales for cartilage [21] and rotator cuff pathologies [22] (1 = no pathology, 2 = superficial or 3 = full-thickness damage of cartilage, labrum, biceps or rotator cuff tendon, severe damage to bone). A senior musculoskeletal radiologist with 12 years of experience in musculoskeletal imaging (T.D.) and blinded to clinical history and FPCT findings evaluated MR arthrography images on all available MR sequences using the same grading scale.

Statistical analysis

All calculations were performed using statistical software (IBM SPSS Statistics, Version 20, IBM, Somer, NY, USA). Descriptive statistics were used for quantitative (mean values and SD) and qualitative data (Median and interquartile range [IQR]).

To detect significant differences between TLD dose and organ dose measurements among different acquisition protocols paired sample Wilcoxon signed rank testing was performed. Confirming normal distribution by Kolmogorov-Smirnov testing, independent (unpaired) samples Student's t-test was performed to detect significant differences between radiation dose of fluoroscopy and arthrography, attenuation values, noise and CNR values between FPCT 5-s and 20-s patient groups. Significant differences between in vivo dose measurements and phantom dose measurements were assessed using Wilcoxon signed rank-sum tests.

Inter-reader agreement for qualitative measures was analyzed by calculating Cohen's kappa (κ) coefficients [23]. Three-point Likert scale ratings of consensus readout data between both readers were dichotomized (1 = negative, 2 and 3 = positive) for calculation of sensitivity, specificity, positive and negative predictive value (PPV and NPV), and accuracy of FPCT arthrography with MR imaging as reference standard. A two-tailed p value of ≤ 0.05 was considered statistically significant with Bonferroni correction for multiple comparisons.

Results

In vitro investigations

Absorbed radiation doses of the different TLDs in the Rand-Alderson phantom and respective CT acquisitions are given in Table 1 with a more detailed description in the Supplemental Material. Calculated organ dose values (mSv) of the right shoulder joint were significantly lower in the FPCT 5-s protocol, as here the midline of the phantom was positioned in the isocentre while in the FPCT 20-s protocol the right shoulder was positioned in the isocentre of the C-arm rotation. Overall, organ dose values in the FPCT 5-s protocol were significantly lower than in the FPCT 20-s protocol, especially in the organs of the neck and thorax (all p-values < 0.05). MDCT was associated with generally higher doses compared to the FPCT 5-s protocol except for brain and thyroid gland ($p = 0.85$ and 0.15) (Table 1). Compared to MDCT the FPCT 20-s protocol applied markedly higher dose in the right shoulder (tenfold), right lung and oesophagus (threefold).

The total effective radiation doses according to ICRP 103 for FPCT 5-s, 20-s and MDCT protocol were 0.6 mSv, 3.4 mSv and 1.7 mSv, respectively.

In vivo investigations

Radiation dose

The radiation doses (accumulated radiation dose at the IRP in mGy and DAP in μGym^2) as given in the respective dose reports of the in vivo shoulder

acquisitions are presented in Table 2. They did not differ significantly from the phantom acquisitions (all $p \geq 0.05$; Table 2).

As seen with the phantom measurements (see above), the radiation dose applied in the FPCT 5-s patient acquisitions was significantly lower than in the FPCT 20-s acquisitions (all $p < 0.001$). Radiation dose of fluoroscopy (used for needle control during injection) did not differ significantly between the two patient groups ($p = 0.189$ and $p = 0.422$ for radiation dose at IRP in mGy and DAP in μGym^2 values, respectively; Table 2).

Quantitative data

Attenuation (in HU) of the different anatomical structures did not vary significantly between the in vivo FPCT 5-s and 20-s acquisitions (all $p \geq 0.05$). However, as expected, noise levels measured in the in vivo FPCT 5-s acquisitions were significantly higher compared to the FPCT 20-s acquisitions (all $p < 0.05$; Supplemental Table 2, Fig. 2).

CNR values of the different joint compartments differed significantly between the in vivo FPCT 5-s and 20-s acquisitions with the latter providing a higher CNR in all compartments (all $p \leq 0.05$; Supplemental Table 2, Fig. 2).

Qualitative data

Inter-reader agreements for the different parameters were moderate to excellent with κ ranging between 0.47 and 1 (Supplemental Table 3).

Technical quality of the intra-articular contrast material injection procedure was generally considered as perfect with no significant differences between the FPCT 5-s and 20-s acquisitions ($p > 0.05$). Subjective image quality of FPCT 20-s acquisitions was rated higher than FPCT 5-s acquisitions (median rating 1 in FPCT 20-s vs. 2 in FPCT 5-s acquisitions), however without reaching statistical significance ($p > 0.05$) (Supplemental Table 3, Fig. 2). Incidences of pathological findings, i.e. findings rated as 2 or 3 on the 3-point Likert scale according to the MR reference standard in the respective FPCT groups (5-s /20-s) were 5/4 (15 %/12 %) for cartilage, 7/16 (21 %/47 %) for bone, 10/16 (20 %/31 %) for labrum or biceps tendon, 5/11 (10 %/22 %) for rotator cuff and 9/4 (53 %/24 %) for AC-joint pathologies.

Sensitivities, specificities, PPV, NPV and accuracies for the consensus data on different joint pathologies in FPCT 5-s and 20-s acquisitions are presented in Table 3 and illustrated in Fig. 3.

Discussion

To the best of our knowledge, this is the first clinical proof-of-concept study on FPCT arthrography of the shoulder in patients, and the first overall presenting in vivo and in vitro data of a thorough radiation dose analysis.

As expected and according to Rando-Alderson phantom measurements using TLDs, the effective dose of the FPCT 5-s protocol was significantly lower than that of the FPCT 20-s protocol with an almost sixfold (3.4 mSv) dose of the latter compared to the FPCT 5-s protocol (0.6 mSv). Dose-wise, the standard MDCT protocol of our institution was in between using almost threefold the radiation dose (1.7 mSv) of the FPCT 5-s protocol. Hence, the FPCT 20-s protocol used a significantly higher radiation dose than the standard MDCT protocol. Importantly, the ex vivo measured radiation dose was similar to that listed by the FPCT unit in vivo. In order to assess the radiation dose of the FPCT protocols appropriately, one needs to keep in mind that dose significantly varies between different systems, depending on the control system of radiation exposure, detector sensitivity as well as the spectrum of the X-ray source.

Table 2 Radiation dose comparisons of FPCT protocols. Comparison between radiation doses acquired in in vivo FPCT shoulder arthrographies and in vitro phantom acquisitions (upper part); comparison between radiation doses of different in vivo FPCT shoulder arthrography protocols (lower part)

	Dose at IRP mGy (± SD)	DAP in μGym^2 (± SD)	Dose at IRP mGy (± SD)	DAP in μGym^2 (± SD)	Dose at IRP mGy (± SD)	DAP in μGym^2 (± SD)
	In vivo Arthrography		Phantom acquisition		Difference; p-value	
FPCT 5 s	56.40 (± 16.61)	857.40 (± 359.39)	34.90 (± N/A)	700.00 (± N/A)	21.5; 0.211	157; 0.526
FPCT 20 s	177.90 (± 51.93)	3196.77 (± 1058.94)	148.00 (± N/A)	4632.00 (± N/A)	29.9; 0.667	1,435.2; 0.381
	In vivo FPCT 5 s		In vivo FPCT 20 s		Mean difference (±SD); p-value	
Arthrography	56.40 (± 16.61)	857.40 (± 359.39)	177.90 (± 51.93)	3,196.77 (± 1058.94)	121.5 (±12.8); 0.000	2,339 (±262.5); 0.000
Fluoroscopy	8.76 (± 7.86)	128.28 (± 137.06)	5.69 (± 5.98)	96.76 (± 101.12)	3.1 (±2.3); 0.189	31.5 (±38.8); 0.422

SD standard deviation, *IRP* interventional reference point, *DAP* dose area product, *FPCT* flat-panel computed tomography

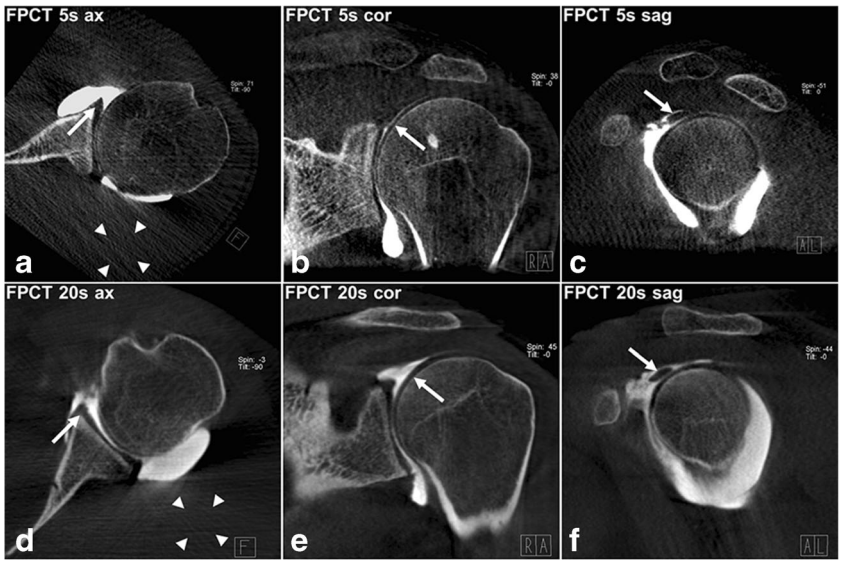

Fig. 2 Twenty-three-year-old male patient with flat panel CT (FPCT) 5-s (**a-c**) and thirty-year-old female patient with FPCT 20-s arthrography of the left shoulder joint (**d-f**): note significantly higher image noise (arrowheads) in FPCT 5 s (**a**) compared to FPCT 20 s (**d**), however with diagnostic image quality in both acquisitions. Arrows indicate intact glenoid labrum (**a** and **d**), humeral cartilage (**b** and **e**) and biceps tendon (**c** and **e**) in respective acquisitions with sharper contours in FPCT 20-s images

Collimation was kept constant for both acquisitions, as it is known to substantially influence image quality and radiation dose [24]. Further, FPCT protocols allowed eccentric rotations of the C-arm gantry around an isocentre located lateral to the table centre (i.e. the shoulder). Consequently, the imaged shoulder received higher radiation dose than the contralateral side. This, however, did not apply to the 5-s protocol in the phantom study, as the rotation centre was the table centre and both shoulders were exposed to approximately the same radiation dose. Yet the organ dose of the shoulders is not considered when calculating the effective dose according to ICRP 103.

Calculated CNR values were all significantly higher in the FPCT 20-s compared to FPCT 5-s acquisitions ,which is consistent with findings of a previous study on CNR dependence on radiation dose in FPCT [25].

Differences between FPCT 5-s and 20-s acquisitions seen in the quantitative measures are moderately reflected in the qualitative ratings. A slight increase in sensitivity for labrum or biceps tendon pathology (40 % vs. 50 %) and a marked increase for cartilage and rotator cuff pathologies (40 % vs. 75 % and 20 % vs. 73 %, respectively) were noted for FPCT 20-s vs. 5-s acquisitions. Although the FPCT 20-s acquisitions delivered better image quality with fewer artifacts, the diagnostic performance for the remainder of joint pathologies with regard to specificity, PPV, NPV and accuracy was comparable to FPCT 5-s acquisition. This corroborates findings of recent studies with excellent image quality for bone visualization using cone-beam CT [26] and good diagnostic performance for cartilage lesions in FPCT using an 8-s intermediate radiation dose protocol [9]. In contrast to published studies on the performance of MDCT arthrography for cartilage and labrum defects of the shoulder [27–31], sensitivity of FPCT was low. Although generally higher in 20-s acquisitions sensitivities for both pathologies amounted to only 75 % and 50 %, well below reported values in MDCT arthrography. A major source for deterioration of image quality are different attenuation profiles and incomplete trajectories of the volume of interests of a 200 ° C-arm rotation around the shoulder joint which can lead to marked truncation artefacts. In addition, as seen in our FPCT arthrograms, potential high spatial resolution of FPCT can be hampered by susceptibility to cone-beam and ring artifacts, decreasing sensitivity for e.g. cartilage and labrum defects. MDCT arthrography of the shoulder is less affected by beam hardening artifacts, although photon starvation in analogy to FPCT is an issue [32]. Additional artifacts may occur when using cone-beam instead of fan-beam geometry [5, 6, 33]. Patients with metallic implants were therefore excluded from this study as this was beyond the scope of this study.

Acquisition duration in FPCT is usually between 5 and 20 s and thus susceptible to movement artifacts. Current MDCT scanners are operating at high pitches, covering the spiral scan-range of a shoulder joint within 2–3 seconds. Further, in contrast to MDCT soft tissue resolution is weak in FPCT [4, 34, 35] and cannot be fully compensated by dedicated convolution kernels. Therefore, as a major drawback quantification of muscle atrophy or fatty replacement is markedly inferior to MDCT or MR imaging. Hence, we reconstructed raw data with high convolution kernels in order to enhance and focus on high density structures like iodine-cartilage or iodine-bone interfaces while compromising soft tissue resolution.

Table 3 Diagnostic performance of FPCT. Diagnostic performance of FPCT 5-s and 20-s arthrographies with MR arthrography as reference standard

	True positives 5 s/20 s	True negatives 5 s/20 s	False positives 5 s/20 s	False negatives 5 s/20 s	Sensitivity [%] 5 s/20 s	Specificity [%] 5 s/20 s	PPV [%] 5 s/ 20 s	NPV [%] 5 s/ 20 s	Accuracy [%] 5 s/20 s
Cartilage pathology	2 / 3	28 / 30	1 / 0	3 / 1	40 / 75	97 / 99	67 / 99	90 / 97	88 / 97
Bone pathology	6 / 13	27 / 14	0 / 4	1 / 3	86 / 81	99 / 78	99 / 76	96 / 82	97 / 79
Labrum or biceps tendon pathology	4 / 9	39 / 28	1 / 2	6 / 9	40 / 50	98 / 93	80 / 82	87 / 76	86 / 77
Rotator cuff pathology	1 / 8	46 / 38	0 / 0	4 / 3	20 / 73	99 / 99	99 / 99	92 / 99	92 / 93
Acromioclavicular- joint pathology	8 / 4	7 / 13	1 / 0	1 / 0	89 / 99	88 / 99	89 / 99	88 / 99	88 / 99

Likert-scale ratings from both FPCT and MR acquisitions were dichotomized with rating 1 = negative, and ratings 2 and 3 = positive for pathology

FPCT flat-panel computed tomography

Our study has several limitations. First, two different FPCT acquisition protocols were compared to one standard MDCT arthrography protocol. Radiation dose values in MDCT arthrography may also be optimized. Second, no surgical or arthroscopic data with intraoperative findings were available in our patients. Last, there were only 34 patients with 17 subjects for each FPCT acquisition. Larger patient cohorts are required in order to further define the clinical impact of FPCT arthrography of the shoulder. A potential role could be in patients with contraindications to both MR (e.g. pacemaker) and CT (e.g. claustrophobia) imaging.

In conclusion using a fast 5-s acquisition, C-arm FPCT shoulder arthrography provides lower radiation doses compared to MDCT arthrography in vitro but poor sensitivity for cartilage and rotator cuff pathologies in vivo. FPCT 20-s protocol is moderately sensitive in vivo for detecting articular and rotator cuff tendon pathology but associated with a markedly higher radiation dose compared to MDCT. Though MR or

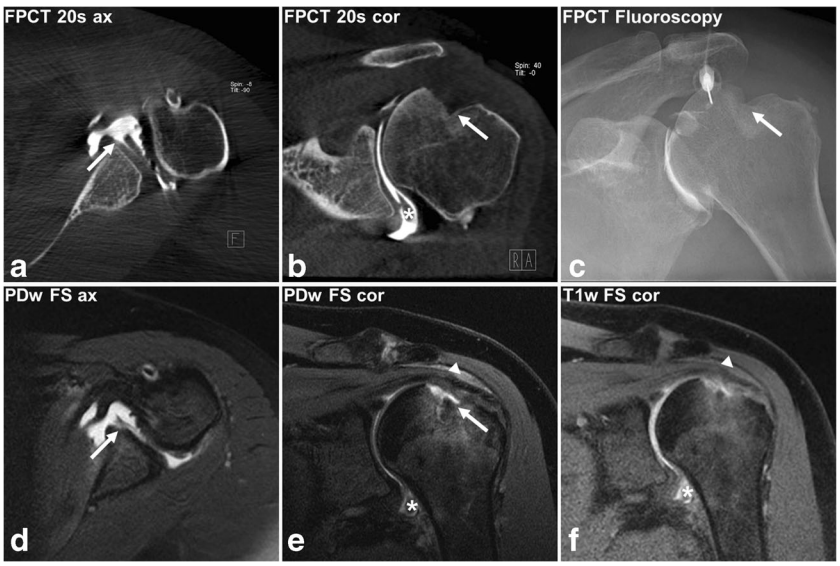

Fig. 3 Fifty-year-old female patient after left antero-inferior shoulder luxation. A marked Hill-Sachs defect of the left humeral head (arrow) can be appreciated already on fluoroscopy (**c**) performed in a C-arm flat panel CT (FPCT) unit, in coronal FPCT 20-s images (**b**) and coronal proton-density weighted fat-saturated (PDw FS) MR-arthrography images (**e**). Adjacent articular sided partial tear of the supraspinate tendon was only seen on MR due to lack of intra-articular contrast in FPCT at this location (cranially adjacent to arrow in **b** and **e**, false-negative finding). Corresponding Bankart-lesion of the antero-inferior labrum can be nicely delineated on both FPCT and axial PDw FS images (in **a** and **d**; true-positive finding). Bursal effusion/hematoma is seen on coronal PDw FS and T1-weighted fat saturated (T1w FS) images of MR-arthrography (arrowheads in **e** and **f**) but without extra-articular contrast leakage indicative of transmural rotator cuff tear. Asterisks in **b**, **e** and **f** mark small intra-articular coagulum, nicely depicted in both modalities

MDCT arthrography enable exact diagnosis of soft tissue pathology, FPCT arthrography may serve as an alternative in instances where MR or MDCT imaging cannot be performed.

Acknowledgments The scientific guarantor of this publication is Prof. Juerg Hodler. The authors of this manuscript declare relationships with the following companies: Rosemarie Scholz, Christoph Koehler and Thilo Elsässer are employees of Siemens Healthcare GmbH, Business Area Advanced Therapies. They were involved in in vitro phantom measurements and data acquisitions but not in in vivo FPCT and MR arthrographies and consecutive data acquisitions. They had no influence on the statistic work-up of the acquired in vivo data.

All the other authors of this manuscript declare no relationships with any companies, whose products or services may be related to the subject matter of the article. This study has received funding by Siemens Healthcare GmbH, Business Area Advanced Therapies and was conducted as part of a collaboration contract with the Institute of Diagnostic and Interventional Radiology of the University Hospital Zurich. One of the authors has significant statistical expertise. Institutional Review Board approval was obtained. Written informed consent was obtained from all subjects (patients) in this study. Methodology: prospective, diagnostic or prognostic study, performed at one institution.

References

1. Lecouvet FE, Simoni P, Koutaissoff S, Vande Berg BC, Malghem J, Dubuc JE (2008) Multidetector spiral CT arthrography of the shoulder. Clinical applications and limits, with MR arthrography and arthroscopic correlations. Eur J Radiol 68:120–136
2. Buckwalter KA (2006) CT Arthrography. Clin Sports Med 25:899–915
3. Farber JM (2004) CT arthrography and postoperative musculoskeletal imaging with multichannel computed tomography. Semin Musculoskelet Radiol 8:157–166
4. Kalender WA, Kyriakou Y (2007) Flat-detector computed tomography (FD-CT). Eur Radiol 17:2767–2779
5. Prokop M (2003) General principles of MDCT. Eur J Radiol 45: S4–S10
6. Neubauer J, Voigt JM, Lang H et al (2014) Comparing the image quality of a mobile flat-panel computed tomography and a multidetector computed tomography: a phantom study. Investig Radiol 49:491–497
7. Penzkofer T, Isfort P, Bruners P et al (2010) Robot arm based flat panel CT-guided electromagnetic tracked spine interventions: phantom and animal model experiments. Eur Radiol 20:2656–2662
8. Guggenberger R, Fischer MA, Hodler J, Pfammatter T, Andreisek G (2012) Flat-Panel CT Arthrography: Feasibility Study and Comparison to Multidetector CT Arthrography. Investig Radiol 47:312–8
9. Chemouni D, Champsaur P, Guenoun D, Desrousseaux J, Pauly V, Le Corroller T (2014) Diagnostic Performance of Flat-Panel CT Arthrography for Cartilage Defect Detection in the Ankle Joint: Comparison With MDCT Arthrography With Gross Anatomy as the Reference Standard. AJR Am J Roentgenol 203:1069–1074
10. Kyriakou Y, Struffert T, Dorfler A, Kalender WA (2009) Basic principles of flat detector computed tomography (FD-CT). Radiologe 49:811–819
11. Sun G, Jin P, Li M, Liu XW, Li FD (2012) Three-dimensional C-arm computed tomography reformation combined with fluoroscopic-guided sacroplasty for sacral metastases. Supportive Care Cancer : Off J Multinatl Assoc Support Care Cancer 20: 2083–2088
12. Tam AL, Mohamed A, Pfister M et al (2010) C-arm cone beam computed tomography needle path overlay for fluoroscopic guided vertebroplasty. Spine 35:1095–1099
13. Ramdhian-Wihlm R, Le Minor JM, Schmittbuhl M et al (2011) Cone-beam computed tomography arthrography: an innovative modality for the evaluation of wrist ligament and cartilage injuries. Skelet Radiol 41:963–969
14. Guggenberger R, Morsbach F, Alkadhi H et al (2013) C-arm flat-panel CT arthrography of the wrist and elbow: first experiences in human cadavers. Skelet Radiol 42:419–429
15. Bai M, Liu B, Mu H, Liu X, Jiang Y (2011) The comparison of radiation dose between C-arm flat-detector CT (DynaCT) and multislice CT (MSCT): A phantom study. Eur J Radiol 81:3577–3580
16. Archer BR, Glaze S, North LB, Bushong SC (1977) Dosimeter placement in the Rando phantom. Med Phys 4:315–318
17. Deak PD, Langner O, Lell M, Kalender WA (2009) Effects of adaptive section collimation on patient radiation dose in multisection spiral CT. Radiology 252:140–147
18. (2007) The 2007 Recommendations of the International Commission on Radiological Protection. ICRP publication 103. Ann ICRP 37(2-4):1-332
19. Ahn SJ, Hong SH, Chai JW et al (2014) Comparison of image quality of shoulder CT arthrography conducted using 120 kVp and 140 kVp protocols. Korean J Radiol 15:739–745
20. Andreisek G, Froehlich JM, Hodler J et al (2008) Direct MR arthrography at 1.5 and 3.0 T: signal dependence on gadolinium and iodine concentrations-phantom study. Radiology 247:706–716
21. Jungius KP, Schmid MR, Zanetti M, Hodler J, Koch P, Pfirrmann CW (2006) Cartilaginous defects of the femorotibial joint: accuracy of coronal short inversion time inversion-recovery MR sequence. Radiology 240:482–488
22. Hodler J, Kursunoglu-Brahme S, Snyder SJ et al (1992) Rotator cuff disease: assessment with MR arthrography versus standard MR imaging in 36 patients with arthroscopic confirmation. Radiology 182:431–436
23. Viera AJ, Garrett JM (2005) Understanding interobserver agreement: the kappa statistic. Fam Med 37:360–363
24. Werncke T, von Falck C, Luepke M, Stamm G, Wacker FK, Meyer BC (2015) Collimation and Image Quality of C-Arm Computed Tomography: Potential of Radiation Dose Reduction While Maintaining Equal Image Quality. Investigative radiology 50: 514–21
25. Guggenberger R, Winklhofer S, Spiczak JV, Andreisek G, Alkadhi H (2013) In vitro high-resolution flat-panel computed tomographic arthrography for artificial cartilage defect detection: comparison with multidetector computed tomography. Investig Radiol 48: 614–621
26. Demehri S, Muhit A, Zbijewski W et al (2015) Assessment of image quality in soft tissue and bone visualization tasks for a dedicated extremity cone-beam CT system. Eur Radiol 25:1742–1751
27. Imhoff AB, Hodler J (1996) Correlation of MR imaging, CT arthrography, and arthroscopy of the shoulder. Bull Hosp Jt Dis 54:146–152
28. Bresler F, Blum A, Braun M et al (1998) Assessment of the superior labrum of the shoulder joint with CT-arthrography and MR-arthrography: correlation with anatomical dissection. Surg Radiol Anat 20:57–62
29. Roger B, Skaf A, Hooper AW, Lektrakul N, Yeh L, Resnick D (1999) Imaging findings in the dominant shoulder of throwing athletes: comparison of radiography, arthrography, CT arthrography, and MR arthrography with arthroscopic correlation. AJR Am J Roentgenol 172:1371–1380
30. Kim YJ, Choi JA, Oh JH, Hwang SI, Hong SH, Kang HS (2011) Superior Labral Anteroposterior Tears: Accuracy and

Interobserver Reliability of Multidetector CT Arthrography for Diagnosis. Radiology 260:207–15

31. Omoumi P, Rubini A, Dubuc JE, Vande Berg BC, Lecouvet FE (2015) Diagnostic performance of CT-arthrography and 1.5T MR-arthrography for the assessment of glenohumeral joint cartilage: a comparative study with arthroscopic correlation. Eur Radiol 25:961–969
32. Mori I, Machida Y, Osanai M, Iinuma K (2013) Photon starvation artifacts of X-ray CT: their true cause and a solution. Radiol Phys Technol 6:130–141
33. Prell D, Kyriakou Y, Kalender WA (2009) Comparison of ring artifact correction methods for flat-detector CT. Phys Med Biol 54:3881–3895
34. Demehri S, Muhit A, Zbijewski W et al (2015) Assessment of image quality in soft tissue and bonevisualization tasks for a dedicated extremity cone-beam CT system. Eur Radiol 25: 1742–1751
35. Lang H, Neubauer J, Fritz B et al (2016) A retrospective, semi-quantitative image quality analysis of cone beam computed tomography (CBCT) and MSCT in the diagnosis of distal radius fractures. Eur Radiol. doi:10.1007/s00330-016-4321-7